

# Training via quantum superposition circumventing local minima and vanishing gradient of sinusoidal neural network.

Zujin Wen\* and Jin-Long Huang\*

*Department of Physics, City University of Hong Kong,  
Tat Chee Avenue, Kowloon, Hong Kong SAR, China*

Oscar Dahlsten†

*Department of Physics, City University of Hong Kong,  
Tat Chee Avenue, Kowloon, Hong Kong SAR, China  
Shenzhen Institute for Quantum Science and Engineering,  
SUSTech, Nanshan District, Shenzhen 518055, China and*

*Institute of Nanoscience and Applications, Southern University of Science and Technology, Shenzhen 518055, China*

(Dated: October 30, 2024)

Deep neural networks have been very successful in applications ranging from computer vision and natural language processing to strategy optimization in games. Recently neural networks with sinusoidal activation functions (SinNN) were found to be ideally suited for representing complex natural signals and their fine spatial and temporal details, which makes them effective representations of images, sound, and video, and good solvers of differential equations. However, training SinNN via gradient descent often results in bad local minima, posing a significant challenge when optimizing their weights. Furthermore, when the weights are discretized for better memory and inference efficiency on small devices, we find that a vanishing gradient problem appears on the resulting discrete SinNN (DSinNN). Brute force search provides an alternative way to find the best weights for DSinNN but is intractable for a large number of parameters. We here provide a qualitatively different training method: an algorithm for quantum training of DSinNNs. The quantum training evolves an initially uniform superposition over weight values to one that is guaranteed to peak on the best weights. We demonstrate the algorithm on toy examples and show that it indeed outperforms gradient descent in optimizing the loss function and outperforms brute force search in the time required.

## I. INTRODUCTION

Neural networks demonstrated exceptional performance across a diverse range of applications, including image classification [1], speech recognition [2], natural language processing [3], autonomous driving [4], and medical diagnostics [5]. Their capability to learn from data has greatly transformed our approach to problem-solving and data analysis [6].

Each layer of a neural network consists of two consecutive operations: linear and nonlinear transformations. Various functions have been used for the nonlinear transformation (called activation function), such as Sigmoid [7], ReLU [8], ELU [9], Leaky ReLU [10], GELU [11], and SiLU [12]. There are also extensive studies using periodic functions as activation. Fourier neural networks incorporate the Fourier transformation into neural networks [13, 14]. Periodic nonlinearities have been used to represent images and sequential data [15–19]. Recently periodic activation functions like *sine* functions have been shown to accurately represent complex natural signals, with wide applications in processing images, sound, and video, and solving differential equations [20]. The representational power of such ac-

tivation functions originates from their capability to model higher-order derivatives of spatial and temporal signals [20].

At the same time, binary neural networks (BNNs) with binary weights and binary activation outputs, are emerging as a noteworthy development due to their hardware efficiency and effectiveness [21–23]. BNNs significantly reduce computational demands and memory usage, making them particularly suitable for deployment in edge devices and resource-constrained environments. BNNs can be seen as a modification of traditional neural networks, designed to maximize efficiency with minimal impact on performance. BNNs are an extreme case of quantized neural networks [24, 25], wherein more than one bit is used to represent an individual weight more generally.

A challenge when training neural networks is that gradient descent often results in suboptimal local minima. Swirszcz et al. [26] investigate the conditions under which local minima arise in neural networks with commonly used activation functions like sigmoid and ReLU. Parascandolo et al. [16] explore shallow local minima problems when using sine activation functions. One way to deal with the local minima problem when learning periodic functions is to add a monotonically varying term in the activation. For example Liu et al. [27] introduce the Snake activation function,  $\text{Snake}_a := x + \frac{1}{a}\sin^2(ax)$ , as an alternative to the pure sine activation function.

While numerous methods exist for training neural networks, integrating quantum techniques into the training

\* These authors contributed equally to this work.

† [oscar.dahlsten@cityu.edu.hk](mailto:oscar.dahlsten@cityu.edu.hk)

process, exploiting quantum superpositions, is emerging as a significant trend. Such efforts can be categorised into quantum training of *quantum* neural nets (QNNs) or *classical* neural nets respectively. QNNs can be thought of as generalising classical neural networks in the same way to how quantum computing generalises classical computing [28–33]. It has been shown that training QNNs with classical optimization loops could be difficult due to barren plateaus in their training landscapes [34]. One way to circumvent this problem is to use quantum optimization methods [35].

Quantum training of *classical* neural nets moreover offers several advantages, including the potential to reduce the number of parameters or iterations required, thereby enabling more efficient training. The trained results can then be directly applied on classical computers, such that quantum computers are not needed during the inference [36]. For example, in [37], the authors use Grover’s search [38] to reduce the query complexity of the classification task. In [39], Grover’s search was used to reduce the number of iterations for reinforcement learning. Particularly relevant to the present work is that [40] provides an algorithm for supervised learning combined with quantum search to find the global optimum of classical binary neural nets (BNNs). These results altogether show that Quantum training opens up new possibilities for enhancing neural network performance and applicability in solving today’s complex challenges.

A key question that arises is whether in practise quantum search training to find the global optimum is needed, or whether gradient descent suffices.

We therefore here aim to directly compare the performance of classical gradient descent based supervised learning of neural nets with that of quantum search training. More specifically, we aim to validate the effectiveness of quantum training in circumventing shallow local minima and vanishing gradient problems that arise from gradient descent training of classical neural networks, demonstrating the superior performance of the quantum approach.

We focus on neural networks with pure sine activation function (SinNN) due to their effectiveness on various applications [20] and due to the ease with which we can manufacture toy examples with local minima (for an alternative approach to construct such toy examples see [26]). We here demonstrate shallow local minima in SinNN loss landscapes, and convergence to suboptimal weights with different weights initialization. Furthermore, we introduce a *discrete* SinNN model with ternary weights and activation (DSinNN). Surprisingly, we find that DSinNNs easily lead to zero gradients such that training via gradient descent cannot find better weights.

We develop an explicit quantum training algorithm for DSinNN (QSinNN). The training starts with an equal superposition of all DSinNN weight values, and then gradually evolves to the best weights with minimum loss based on Grover’s search. The marking of the good elements during the search is done via quantum phase estima-

tion [41] for turning the training data into a quantum unitary – the oracle unitary of the quantum search. The algorithm is analytically guaranteed to obtain a global minimum with high probability [42]. We simulate QSinNN’s performance on a toy DSinNN model and find that it successfully circumvents numerous local minima and vanishing gradient regions, attaining the global minimum. We have thus, via SinNN and DSinNN, created a scenario where a quantum search training approach similar to [40] can be directly compared with classical training. The direct comparison demonstrates that the QSinNN training demonstrably outperforms gradient descent in reducing the loss and achieves better time complexity than brute force search for these important neural nets.

## II. CLASSICAL SINUSOIDAL NEURAL NETWORKS AND THEIR TRAINING

In this section, we first describe classical sinusoidal neural networks and how we discretise them. We then demonstrate two issues with gradient descent training methods of these networks: bad local minima and vanishing gradients.

### A. Classical discrete sinusoidal neural networks

A sinusoidal Neural Network (SinNN) uses the sine function as an activation function[20]. The output  $z'_j$  of a layer of neurons is obtained from inputs  $z_i$  by

$$z'_j = \sin \sum_i (w_{ij} \cdot z_i). \quad (1)$$

In general the output  $\hat{y}$  can be a non-linear function of the previous layer’s outputs, like softmax, but here for simplicity we simply add those outputs.

Binary Neural Networks (BNNs) [21] are a class of neural networks where the weights and activated values of neurons are constrained to binary values (e.g. -1 and 1). We adopt a similar discretization procedure as in [21] for the SinNN model. The new model is called DSinNN. For each hidden layer of DSinNN, inputs  $z_i$  are, in the forward pass, transformed into output  $z'_j$  according to

$$z'_j = D \left( \sin \sum_i (\lambda D(w_{ij}) \cdot z_i) \right), \quad (2)$$

where

$$D(x) \equiv \text{sign}(x) = \begin{cases} -1 & \text{if } x < 0 \\ 0 & \text{if } x = 0 \\ 1 & \text{if } x > 0, \end{cases}$$

$w_{ij}$  is real-valued, and  $\lambda$  is 1 for the first hidden layer and  $\frac{\pi}{2^n}$  for some fixed integer  $n$  for deeper hidden layers. The introduced  $\lambda$  simplifies our discussion of one hidden layer DSinNN.

The Mean Square Error is used as the loss function to update weights. However, since the gradient of the sign function is zero almost everywhere, back-propagated errors will also be zero almost everywhere. To avoid this obstacle, the Straight-Through Estimator (STE) was proposed in [21] to let back-propagation bypass the discretization procedure, such that real-valued weights could be properly updated in the training process. In this paper, we choose an identity function  $f(x) = x$  for STE for simplicity, instead of the hardtanh used in [21].

### B. Bad local minima in SinNN

We develop a toy model to demonstrate the bad local minima phenomenon in SinNN, as shown in Figure 1a. The toy model only has one scalar input and one scalar output with one hidden layer of two neurons. For each input  $x$ , model output is  $\hat{y} = \sin(w_1x) + \sin(w_2x)$ .

The toy model is trained with four input-output pairs in a single batch. Thus the MSE loss averaged over this batch is  $\frac{1}{4} \sum_1^4 (y_i - \hat{y}_i)^2$ , where the index  $i$  is over samples in the batch. Four input-output pairs  $(x_i, y_i)$  are generated by the target function  $y = \sin(1 \cdot x) + \sin(1 \cdot x)$ :

$$\left(-\frac{3\pi}{2}, 2\right), \left(-\frac{\pi}{2}, -2\right), \left(\frac{\pi}{2}, 2\right), \left(\frac{3\pi}{2}, -2\right).$$

Thus, the optimal weights are  $(w_1, w_2) = (1, 1)$ .

The contour plot of the loss landscape is presented in Figure 1b. White regions are mountains with a loss greater than 5, and darker regions are valleys corresponding to a smaller loss. From the plot, we can observe 8 shallow valleys where the surrounding areas are higher, clearly indicating that these valleys are local minima, and only one global minimum exists, at location (1, 1). Moreover, since the sine function is periodic, local minima will arise periodically, meaning that they can be found throughout the landscape.

In Figure 1c, we plot the loss as a function of the number of epochs for 20 different initial weights. In most cases, the weights get stuck at local minima with higher loss than the global minimum. In this situation, gradient descent has great difficulty in training neural networks to reach global minima.

### C. Vanishing Gradients in DSinNN

A toy model for DSinNN is shown in Figure 2a.  $w_1, w_2$  are two real trainable parameters. Given input  $x$ , the model output is

$$z_i = D(\sin(D(w_i) \cdot x)), \quad i = 1, 2, \quad (3)$$

$$\hat{y} = D(z_1 + z_2). \quad (4)$$

Batch mean MSE is used as a loss function, as in SinNN. The target output function is  $y = D(D(\sin(1 \cdot x)) + D(\sin(1 \cdot x)))$ . The four training data points we will use are

$$\left(-\frac{3\pi}{2}, 1\right), \left(-\frac{\pi}{2}, -1\right), \left(\frac{\pi}{2}, 1\right), \left(\frac{3\pi}{2}, -1\right).$$

The optimal weight configuration should satisfy  $\{(w_1, w_2) | w_1 > 0, w_2 > 0\}$ .

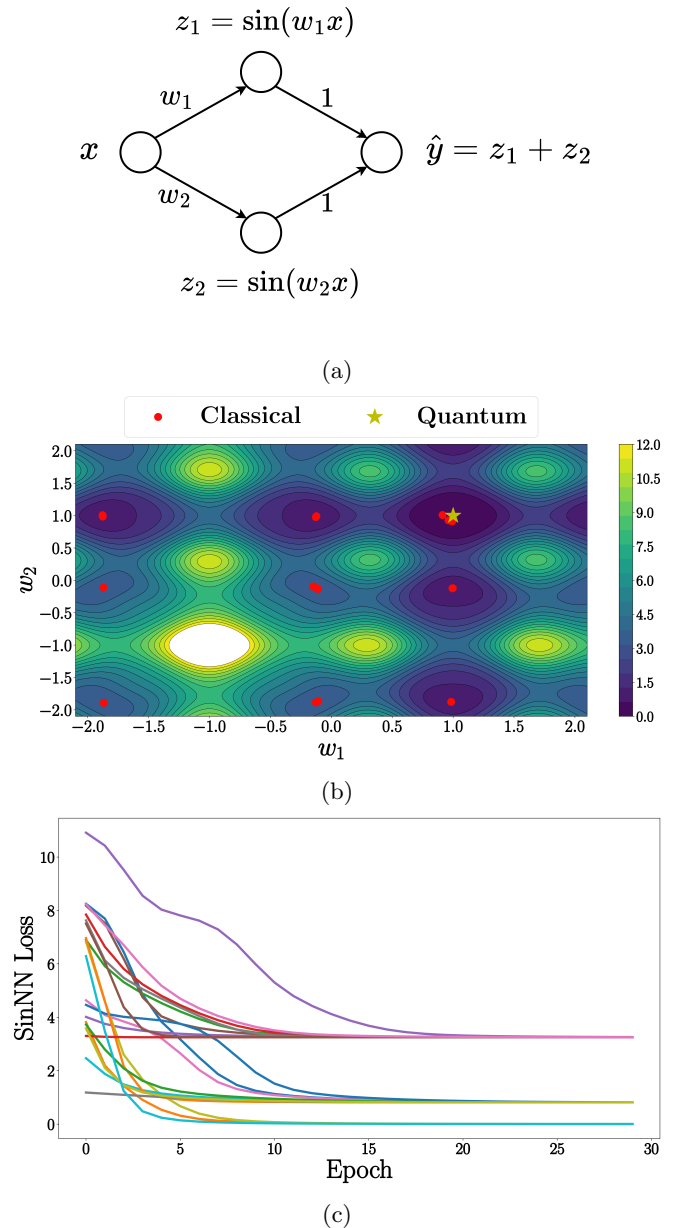


FIG. 1: **Training of toy SinNN model.** (a) A SinNN with only two trainable parameters  $w_1, w_2$ . (b) Loss landscape for SinNN. The white regions' losses are greater than 12. There is 1 global minimum and 8 local minima in the figure. (c) Loss history for classical training of SinNN as a function of epochs for 20 different initial weights. Most of the lines do not reach the global minimum.

Figure 2b is the loss landscape for the toy DSinNN model. Only the first quadrant is the global minimum.

The other three quadrants are barren plateaus. [Figure 2c](#) plots loss as a function of epochs for 20 different randomly initialized weights. Losses are perturbed by a small random amount to distinguish lines with different initial weights. Weights that started in regions with higher loss do not move to regions with lower loss.

Note that although the loss landscape for DSinNN appears flat in each region, the gradients of loss with respect to parameters  $w_1, w_2$  are usually nonzero, due to the usage of STE. In general the loss  $L = \frac{1}{N} \sum_x (\hat{y}_x - y_x)^2$ . The gradient is

$$\frac{\partial L}{\partial w_i} = \frac{1}{N} \sum_x 2 \cdot (\hat{y}_x - y_x) \frac{\partial \hat{y}_x}{\partial w_i}. \quad (5)$$

When calculating  $\frac{\partial \hat{y}_x}{\partial w_i}$ , the discretization function  $D(x)$  is treated as STE identity function  $f(x) = x$ . For example, in our toy DSinNN model,

$$\frac{\partial \hat{y}_x}{\partial w_i} = \cos(D(w_i)x) \cdot x, \quad i = 1, 2. \quad (6)$$

When  $x$  is an integer multiplied by  $\pi/2$ , the gradients for the toy model become zero. For those scenarios, weights are stuck at their initial locations, no matter what their losses are.

The gradient in [Eq. \(5\)](#) differs from the gradient in SinNN since the calculations of  $\hat{y}_x$  are different. Our current definition of DSinNN uses 1 bit to represent each weight. For higher  $n$ -bit representation, its training behavior will be more similar to the training behavior in SinNN, since the loss landscape of DSinNN will be an approximation of that of SinNN if the discretization procedure is chosen appropriately.

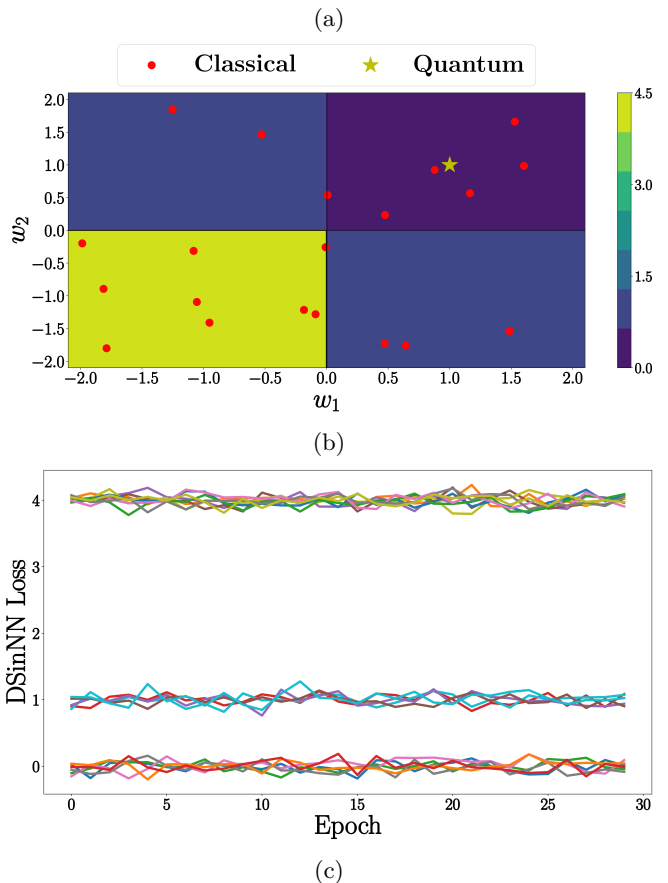
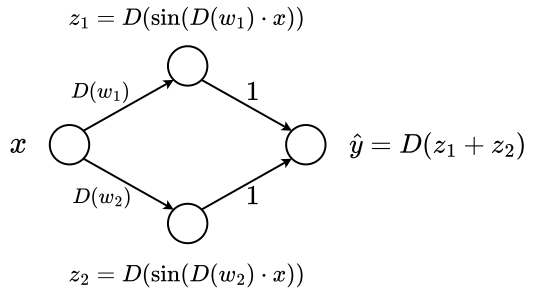


**FIG. 2: Training of toy DSinNN model.** (a) A DSinNN with only two trainable parameters  $w_1, w_2$ .  $D$  is the sign function for discretization. (b) Loss landscape for DSinNN. There are four flat regions and only the first quadrant is the global minimum. (c) Loss history for DSinNN as a function of epochs for 20 different initial weights. A small random number is added to the loss to distinguish lines with different weights initialization. The majority of weight configurations are stuck in regions with higher loss.

### III. QUANTUM TRAINING ALGORITHM FOR DSINNN (QSINNN)

The procedures of the quantum learning algorithm are illustrated in [Figure 3](#) and [Figure 4](#), and proceed as follows:

1. **Create a uniform superposition of weights.** Each weight register represents one trainable parameter in the classical DSinNN model. The weights are initialized in the state  $|0\rangle^{\otimes n}$  and transformed by Hadamard gates into  $|+\rangle^{\otimes n}$ , where  $|+\rangle = \frac{1}{\sqrt{2}}(|0\rangle + |1\rangle)$ , where  $n$  is the number of weight qubits.
2. **Entangle weight registers with phase registers via phase estimation.** The number of phase registers depends on the precision required to distinguish best weight values from other weight values. The unitary operator used in phase estimation simulates the forward passes of classical DSinNN on all training data pairs. Explicitly,  $U = U_N \cdots U_2 U_1$ , where  $N$  is the number of training data pairs. [Figure 4](#) describes each  $U_i, i = 1, 2, \dots, N$  in the following steps:
  - (a)  $\text{Enc}_{x_i}, \text{Enc}_{y_i}$  encode the  $i$ -th input and target into corresponding quantum states. Encoding details are described in [Section A](#).
  - (b) Multiplication of weight and input is implemented through a controlled sign gate, i.e. sign qubit of input is flipped if and only if the controlling weight qubit is in state  $|1\rangle$ .
  - (c) Quantum plus gate and quantum sine gate simulate the classical addition of weighted inputs and the classical sine function. Details are described in [Section B](#) and [Section C](#). The final output is a quantum state of the DSinNN predicted value. These three steps (a)-(c) constitute a quantum forward pass for  $i$ -th training data pair, denoted as  $FF_i$ .
  - (d) Compare quantum forward pass outputs with target registers through a quantum checker gate  $\phi$ . For details see [Section D](#).
  - (e) Apply inverse of quantum forward pass  $FF_i^{-1}$ .
3. **Apply the oracle unitary  $O_{\pm}$  to invert the amplitudes.** This operation inverts the amplitudes of entangled weight states according to phase registers. Further details are provided in [Section E](#).
4. **Disentangle weight registers from others by inverse of phase estimation  $PE^{-1}$ .** This resets all registers to zero states except weight registers. Therefore weight registers are disentangled from the rest, ending in a pure state.

5. **Apply diffusion operator  $D$  on weight registers.**

$$D = H^{\otimes n} (2|0^n\rangle\langle 0^n| - I_n) H^{\otimes n}, \quad (7)$$

It increases amplitudes of “good” weight states.

6. **Steps 2 to 5 are repeated several times.** The final weight states are guaranteed to reach the optimal ones with a high probability [42].

#### A. Quantum encoding of classical data

In this subsection, we describe how to encode classical data into quantum states, i.e. the Enc gates in [Figure 4](#). We consider cases when every input  $x$  can be written in the following form:

$$x = k \cdot \frac{\pi}{2^n}, \quad k \in \mathbb{Z}, \quad n \in \mathbb{N}. \quad (8)$$

Given a whole dataset, a fixed integer  $n$  is chosen as the smallest natural number such that for each input  $x$  there exists an integer  $k$  satisfying Eq. (8). For any integer  $k$  except 0, it satisfies:

$$k = (-1)^{\frac{1 - \text{sign}(k)}{2}} \sum_{i=0}^{m-1} b_i 2^i, \quad b_i \in \{0, 1\}, \quad m \in \mathbb{N}. \quad (9)$$

Hence any nonzero integer  $k$  corresponds to a unique bit string  $b_{\text{sign}} b_{m-1} b_{m-2} \cdots b_0$ , where  $b_{\text{sign}} = \frac{1 - \text{sign}(k)}{2} \in \{0, 1\}$ . The number of qubits to encode  $|k|$  is  $m = \max\{\lceil \log_2 |k|_{\max} \rceil, n\}$ , where  $|k|_{\max}$  is the largest  $|k|$  for all input data. The quantum state  $|\psi_x\rangle$  encoding classical input  $x$  is just a pure state of  $m+1$  qubits:

$$|\psi_x\rangle = |b_{\text{sign}} b_{m-1} b_{m-2} \cdots b_0\rangle. \quad (10)$$

$|\psi_x\rangle$  can be easily created by applying Pauli X gates to  $|0\rangle^{\otimes m+1}$ . When input  $x = 0$ , its quantum encoding  $|\psi_x\rangle$  could be either  $|000 \cdots 0\rangle$  or  $|100 \cdots 0\rangle$ .

We give an example to illustrate the quantum encoding of input. Consider input  $x = \frac{9\pi}{8}$ .

$$\begin{aligned} n &= \log_2 8 = 3, \\ m &= \max\{\lceil \log_2 9 \rceil, n\} = 4, \\ b_{\text{sign}} &= \frac{1 - \text{sign}(9)}{2} = 0, \\ 9 &= 1 \cdot 2^3 + 0 \cdot 2^2 + 0 \cdot 2^1 + 1 \cdot 2^0. \end{aligned}$$

Finally we get  $|\psi_x\rangle = |01001\rangle$ .

Since the target  $y$  is an output of the sign function,  $y \in \{-1, 0, 1\}$ . Its quantum encoding is straightforward:

$$|\psi_y\rangle = \begin{cases} |01\rangle & \text{if } y = 1 \\ |00\rangle & \text{if } y = 0 \\ |11\rangle & \text{if } y = -1, \end{cases} \quad (11)$$

where the first qubit represents the sign of  $y$  and the second qubit represents the value of  $y$ .  $|\psi_y\rangle$  can also be easily prepared using Pauli X gates.

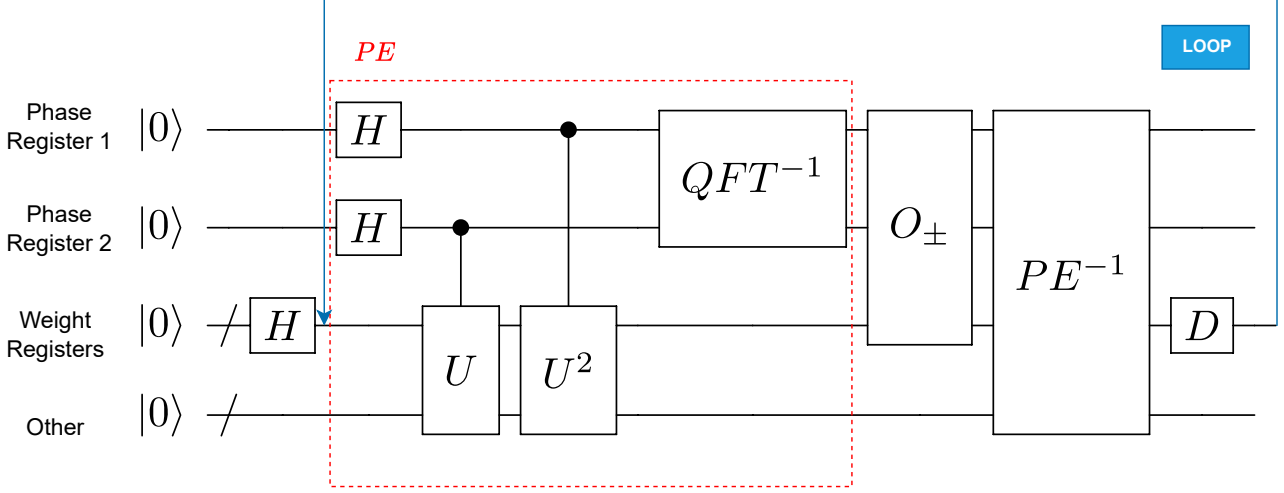


FIG. 3: **Quantum training for DSinNN (QSinNN).**  $PE$  is phase estimation, which we illustrate with two phase registers.  $O_{\pm}$  is the oracle unitary, which changes amplitudes of states from 1 to 1 or -1.  $D$  is the diffusion operator which amplifies “good” weight states.

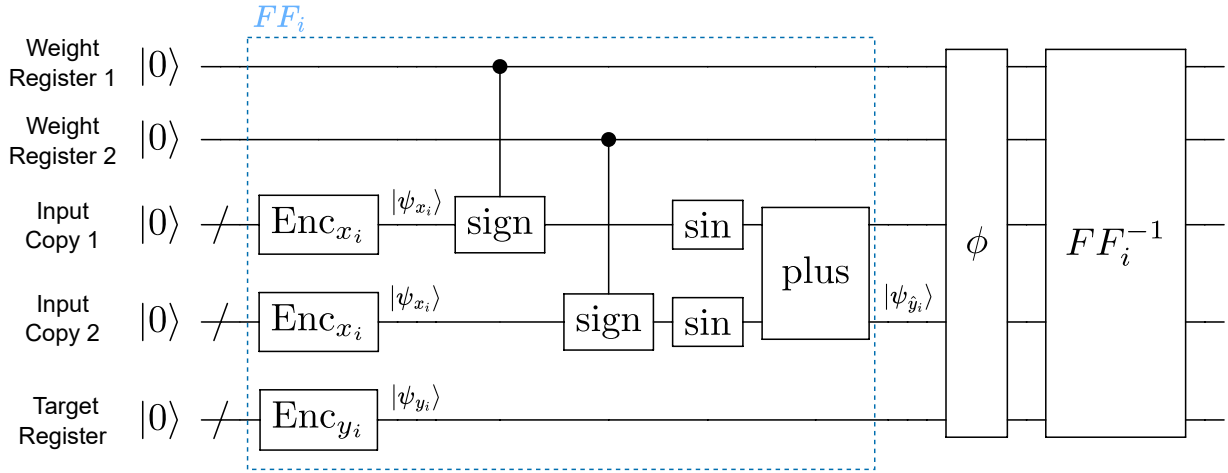


FIG. 4:  $U_i$  used in unitary  $U$  of phase estimation.  $U = U_N \cdots U_2 U_1$ , where  $N$  is the number of training data pairs.  $Enc_{x_i}, Enc_{y_i}$  are Pauli  $X$  gates to prepare input and target states. The controlled sign gate flips the sign qubit of input qubits if and only if the control qubit is  $|1\rangle$ . The number of copies of input states is the same as the number of hidden neurons.  $\sin$ ,  $\text{plus}$ , and  $\phi$  are the quantum  $\sin$ ,  $\text{plus}$ , and checker gates, whose ancilla qubits are omitted in the drawing.  $FF_i$  stands for feed-forward unitary for the  $i$ -th training data pair.

## B. Quantum sine gate

Here we describe the quantum circuit to simulate the classical sine function followed by the discretize function, i.e.  $D(\sin(z))$ , where  $z$  is the input to the hidden neuron in the classical DSinNN model. Note that this gate is a unitary for a classical nonlinear activation function. Its implementation is illustrated in Figure 5. This quantum sine gate realizes the following mapping of quantum

states:

$$|\psi_z\rangle \otimes |0\rangle^{\otimes 2} \mapsto |\psi_z\rangle \otimes |\alpha_{\text{sign}}\rangle \otimes |\alpha_{\text{value}}\rangle, \quad (12)$$

where

$$|\psi_z\rangle = |b_{\text{sign}} b_{m-1} b_{m-2} \cdots b_0\rangle, \quad (13)$$

$$|\alpha_{\text{sign}}\rangle = |b_{\text{sign}} \oplus b_n\rangle, \quad (14)$$

$$|\alpha_{\text{value}}\rangle = |b_0 \vee b_1 \vee \cdots \vee b_{n-1}\rangle. \quad (15)$$

Here  $|\psi_z\rangle$  is the quantum encoding of classical input to the neuron. It has one qubit representing the sign of  $z$

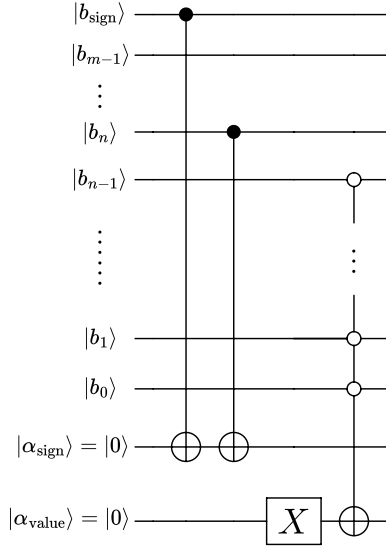


FIG. 5: **Quantum sine gate.** It simulates the classical function  $D(\sin(z))$ , assuming  $m > n$ .  $|\psi_z\rangle = |b_{\text{sign}}b_{m-1}b_{m-2}\cdots b_0\rangle$  is the quantum encoding of  $z$ .  $|\alpha_{\text{sign}}\rangle \otimes |\alpha_{\text{value}}\rangle$  is the final output representing  $D(\sin(z))$ .  $|\psi_z\rangle$  is discarded after this operation.

and  $m+1$  qubits representing the value of  $z$ , as described in Section A.  $\oplus$  is addition module 2 and  $\vee$  is the boolean OR operator. An explanation for the quantum sine gate construction is that:

$$|z| = \sum_{j=n}^{m-1} b_j 2^j \cdot \frac{\pi}{2^n} + \sum_{i=0}^{n-1} b_i 2^i \cdot \frac{\pi}{2^n} \quad (16)$$

$$= q\pi + r, \quad q \in \mathbb{N}, \quad r \in \mathbb{R},$$

where  $r$  represents the portion of  $|z|$  that is smaller than  $\pi$ . Therefore, for  $D(\sin(z))$ , if  $r \neq 0$ , then  $|D(\sin(z))| = 1$ . Equivalently, if  $|b_{n-1}\cdots b_2b_1\rangle \neq |0\cdots 00\rangle$ , then  $|\alpha_{\text{value}}\rangle = |1\rangle$ . The bit  $b_n$  determines whether  $q$  is an odd or even number, and together with  $b_{\text{sign}}$ , it finalizes the sign of  $D(\sin(z))$ , denoted by  $|\alpha_{\text{sign}}\rangle$ .  $|\psi_z\rangle$  can be discarded after this quantum sine gate.  $|\alpha_{\text{sign}}\rangle \otimes |\alpha_{\text{value}}\rangle$  represents  $D(\sin(z))$  and is kept for following processes.

### C. Quantum plus gate

Quantum plus gate simulates  $D(\sum_i z_i)$ , where  $z_i$  is the output of the  $i$ -th hidden neurons. In Figure 4, it is denoted as ‘plus’ gate. Since  $z_i$  is one of  $\{-1, 0, 1\}$ , its corresponding quantum state only needs two registers: one for its sign and one for its value.

$$|\psi_{z_i}\rangle = |\alpha_{is}\rangle \otimes |\alpha_{iv}\rangle. \quad (17)$$

The quantum plus gate consists of two steps:

1. Encode number of states  $|01\rangle, |11\rangle$  in  $\{|\psi_{z_i}\rangle, i = 1, 2, \dots\}$  in registers  $|p\rangle$  and  $|n\rangle$ . Essentially  $p$  is the

number of positive  $z_i$  and  $n$  is the number of negative  $z_i$ . We implement it using quantum adders.

2. Use a quantum comparator [43] to compare  $|p\rangle$  and  $|n\rangle$ . If  $p > n$ , output is  $|01\rangle$ . If  $p < n$ , output is  $|11\rangle$ . Otherwise output is  $|00\rangle$ .

Figure 6 illustrates two quantum half adders to implement step 1 for  $|\psi_{z_1}\rangle = |\alpha_s\rangle \otimes |\alpha_v\rangle$  and  $|\psi_{z_2}\rangle = |\alpha'_s\rangle \otimes |\alpha'_v\rangle$ . The output is  $|p_1p_0\rangle \otimes |n_1n_0\rangle$ .

$$|p_1p_0\rangle = \begin{cases} |00\rangle & \text{if } |\psi_{z_1}\rangle \neq |01\rangle \text{ and } |\psi_{z_2}\rangle \neq |01\rangle, \\ |01\rangle & \text{if } |\psi_{z_1}\rangle = |01\rangle \text{ xor } |\psi_{z_2}\rangle = |01\rangle, \\ |10\rangle & \text{if } |\psi_{z_1}\rangle = |\psi_{z_2}\rangle = |01\rangle. \end{cases} \quad (18)$$

$$|n_1n_0\rangle = \begin{cases} |00\rangle & \text{if } |\psi_{z_1}\rangle \neq |11\rangle \text{ and } |\psi_{z_2}\rangle \neq |11\rangle, \\ |01\rangle & \text{if } |\psi_{z_1}\rangle = |11\rangle \text{ xor } |\psi_{z_2}\rangle = |11\rangle, \\ |10\rangle & \text{if } |\psi_{z_1}\rangle = |\psi_{z_2}\rangle = |11\rangle. \end{cases} \quad (19)$$

If more  $|\psi_{z_i}\rangle$  are involved in step 1, additional quantum full adders are needed. These can be constructed easily through combinations of quantum half adders.

Figure 7a demonstrates a quantum comparator [43] for inputs  $|p_i\rangle$  and  $|n_i\rangle$ . Output  $|q_1q_2\rangle$  satisfies

$$|q_1q_2\rangle = \begin{cases} |11\rangle & \text{if } n_i > p_i, \\ |00\rangle & \text{if } n_i = p_i, \\ |01\rangle & \text{if } n_i < p_i. \end{cases} \quad (20)$$

Figure 7b demonstrates a quantum comparator [43] for inputs  $|p_1p_0\rangle$  and  $|n_1n_0\rangle$ . Output  $|\hat{y}_s\hat{y}_v\rangle$  satisfies

$$|\hat{y}_s\hat{y}_v\rangle = \begin{cases} |11\rangle & \text{if } 2n_1 + n_0 > 2p_1 + p_0, \\ |00\rangle & \text{if } 2n_1 + n_0 = 2p_1 + p_0, \\ |01\rangle & \text{if } 2n_1 + n_0 < 2p_1 + p_0. \end{cases} \quad (21)$$

$|\hat{y}_s\hat{y}_v\rangle$  represents  $|\psi_{\hat{y}_i}\rangle$  in Figure 4.

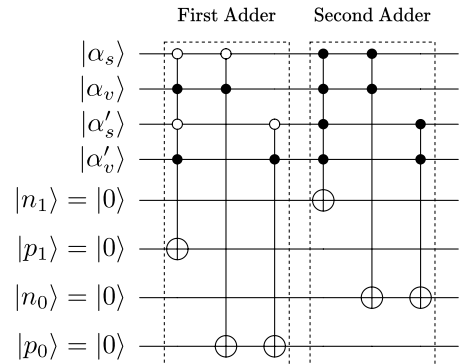


FIG. 6: **Two quantum half adders.** Inputs are  $|\psi_{z_1}\rangle = |\alpha_s\rangle \otimes |\alpha_v\rangle$  and  $|\psi_{z_2}\rangle = |\alpha'_s\rangle \otimes |\alpha'_v\rangle$ . First adder counts the number of  $|01\rangle$  in  $|\psi_{z_1}\rangle$  and  $|\psi_{z_2}\rangle$  into  $|p_1p_0\rangle$ . Second adder counts the number of  $|11\rangle$  in  $|\psi_{z_1}\rangle$  and  $|\psi_{z_2}\rangle$  into  $|n_1n_0\rangle$ .

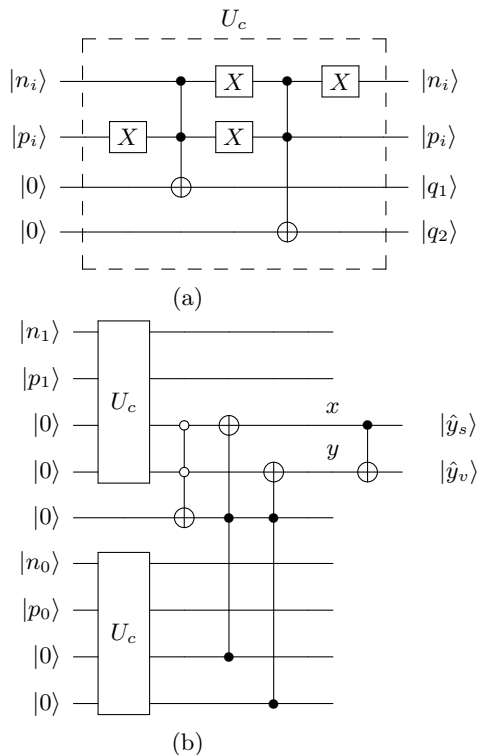


FIG. 7: **Quantum Comparators.** (a) A 1-bit comparator gate  $U_c$ .  $|q_1q_2\rangle = |10\rangle$  if  $n_i > p_i$ .  $|q_1q_2\rangle = |00\rangle$  if  $n_i = p_i$ .  $|q_1q_2\rangle = |01\rangle$  if  $n_i < p_i$ . (b) A 2-bit comparator gate we use in this work.  $|\hat{y}_s\hat{y}_v\rangle$  can be one of  $\{|11\rangle, |00\rangle, |01\rangle\}$  depending on the relation between  $2n_1 + n_0$  and  $2p_1 + p_0$ , as shown in Eq. (21).

#### D. Quantum checker gate

Quantum checker gate checks if the model output  $|\psi_{\hat{y}}\rangle = |\hat{y}_s\hat{y}_v\rangle$  is the same as the target output  $|\psi_y\rangle = |y_sy_v\rangle$  by comparing each qubit through  $U_s$  and  $U_v$ . If so, weight register 1 is rotated by phase angle  $\frac{\pi}{N}$ , where  $N$  is the number of training data pairs. It is drawn as  $\phi$  in Figure 4 and its implementation is given in Figure 8. The checker gate does not affect other weight registers except weight register 1.

If weight states produce correct predictions for all training data, its phase would be  $e^{i\pi} = -1$ . The phase angle for the weight state is larger if the corresponding model outputs have more correct predictions.

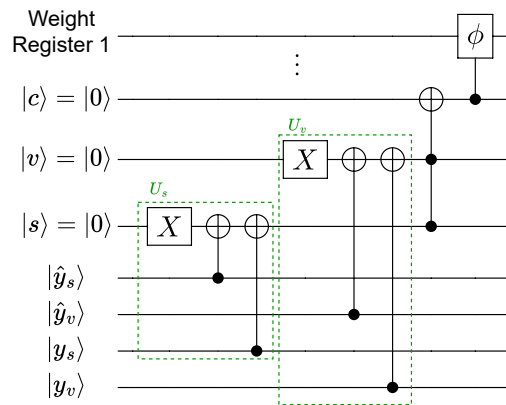


FIG. 8: **Quantum checker gate.** It checks whether  $|\hat{y}_s\rangle = |y_s\rangle$  and  $|\hat{y}_v\rangle = |y_v\rangle$ . If so, a phase shift  $\frac{\pi}{N}$  will be given to weight register 1, where  $N$  is the number of training data pairs.

#### E. Oracle gate

The weights with the phase shift close to  $\pi$  will be considered as the optimal weights. After phase estimation, the information about phase shift moves to phase registers. The oracle gate  $O_{\pm}$  in Figure 4 shifts phases of optimal weight states by an exact angle  $\pi$  according to coupled phase registers.

More specifically, after phase estimation, phase registers  $|j_1j_2 \dots j_{N'}\rangle$  represent the estimated state that previously held a phase of  $2\pi j = 2\pi(j_1/2 + j_2/4 + \dots + j_{N'}/2^{N'})$ . If the phase is greater than a predefined threshold  $2\pi\tau$ :

$$O_{\pm}|j_1j_2 \dots j_{N'}\rangle = \begin{cases} -|j_1j_2 \dots j_{N'}\rangle, & \text{if } j \geq \tau \\ |j_1j_2 \dots j_{N'}\rangle, & \text{otherwise} \end{cases} \quad (22)$$

### IV. NUMERICAL DEMONSTRATION OF QUANTUM TRAINING ADVANTAGE

#### A. Simulation specifics

To enable a direct comparison with the classical training, the same dataset of input-label pairs  $(x_i, y_i)$  used in the DSinNN training of the toy DSinNN model described in Figure 2a is used for the quantum training:

$$\left(-\frac{3\pi}{2}, 1\right), \left(-\frac{\pi}{2}, -1\right), \left(\frac{\pi}{2}, 1\right), \left(\frac{3\pi}{2}, -1\right).$$

The input data  $x_i$  is encoded into three qubits as state  $|\psi_{x_i}\rangle$ , following Equation 8 and Equation 9. Since one  $x_i$  is fed to two neurons, as in Figure 2a, the total number of qubits representing the input is  $n_{\text{input}} = 2 \times 3 = 6$ .

Subsequently, the two copies of  $|\psi_{x_i}\rangle$ , separately pass through sign gates controlled by weight registers, quantum sine gates, and then get combined by the quantum plus gate to output a 2-qubit prediction  $|\psi_{\hat{y}_i}\rangle$ .

The quantum plus gate in [section III C](#) is implemented using a predefined summation matrix. For example, the sum of two 2-qubit binary numbers is expressed as a 3-qubit binary number, and this matrix maps each possible summation result by the multiplication with a  $7 \times 7$  matrix. The dimension 7 is derived from  $2 \times 2 + 3 = 7$ . The subsequent discretization of this sum is determined by the 3-qubit sum's sign and value.

For the comparison between output  $|\psi_{y_i}\rangle$  and target data  $|\psi_{y_i}\rangle$ , we use two qubits to encode the target data as in [Eq. \(11\)](#) and three ancilla qubits to assist comparing the output and target data qubit by qubit. Weight states are assigned a phase shift of  $\frac{\pi}{4}$  each time the corresponding model outputs correctly, as previously stated in [section III D](#). We use two phase estimation qubits for phase registers, which precisely estimates phase values from the set  $\{0, \frac{\pi}{2}, \pi, \frac{3\pi}{2}\}$ .

The total circuit involves 18 qubits as follows:  $n_{\text{PE}} = 2$  phase estimation;  $n_{\text{weight}} = 2$  for weight states;  $n_{\text{input}} = 6$  for input data and its copy (we simplified the implementation of quantum sine gates so that it does not need ancilla qubits—see code for details);  $n_{\text{sum}} = 3$  for summation of two discrete sine results (the discrete binary output can be computed from the summation matrix);  $n_{\text{target}} = 2$  for target data;  $n_{\text{ancilla}} = 3$  for checking whether the output is consistent with the target. In total,  $n_{\text{total}} = n_{\text{PE}} + n_{\text{weight}} + n_{\text{input}} + n_{\text{sum}} + n_{\text{target}} + n_{\text{ancilla}} = 18$ .

We use the QuTiP toolbox [\[44\]](#) to build up the quantum circuit for simulation. The corresponding circuit to realize the quantum training described above is shown in the Supplementary Material.

## B. Results

The weight state  $|00\rangle$  correctly reproduces all four target data and while the other three weight states reproduce none of the target data. Thus  $|00\rangle$  should accumulate a phase shift of  $\pi$ , and the other weight states should accumulate zero phase shift.

The QuTiP simulation shows that, after phase estimation, the density matrix of the phase registers becomes  $\text{diag}(0.75, 0.00, 0.25, 0.00)$ . To interpret this result, recall that the superposition states of the two phase registers can be denoted as  $|j_1 j_2\rangle$ , and the phases are represented as  $2\pi j$ , with  $j = 0, j_1 j_2 = j_1/2 + j_2/4$ , where  $j_i \in \{0, 1\}$ . Thus the phase register density matrix shows that one weight gains  $(2\pi) \times (1 \times \frac{1}{2} + 0 \times \frac{1}{4}) = \pi$  phase shift and the other three weight states gain zero phase shift. Then we set our correctness threshold (described in [section III E](#)) to 4, corresponding to phase threshold  $4 \times \frac{\pi}{4} = \pi$ , which in this case acts trivially, retaining the exact  $\pi$  phase shift of the correct weight state.

After uncomputing the circuit above to disentangle the weight state from the other qubits, the weight state den-

sity matrix is:

$$\begin{bmatrix} 0.25 & -0.25 & -0.25 & -0.25 \\ -0.25 & 0.25 & 0.25 & 0.25 \\ -0.25 & 0.25 & 0.25 & 0.25 \\ -0.25 & 0.25 & 0.25 & 0.25 \end{bmatrix}.$$

That density matrix shows that only  $|00\rangle$  gains a -1 factor as desired.

After the subsequent diffusion operator,  $H^{\otimes n}(2|0\rangle\langle 0| - I)H^{\otimes n}$ , where  $n$  is the number of weight qubits, the final density matrix for the weight qubits becomes  $\text{diag}(1, 0, 0, 0)$ . Therefore the weight state chosen is indeed  $|00\rangle$  as desired. That weight state does not flip the sign of input data, corresponding to classical  $w_1 = 1$  and  $w_2 = 1$ . Thus the quantum training succeeded in finding the global optimum. [Figure 1b](#) and [Figure 2b](#) depict the successful quantum training outcome and contrast it with the classical training outcome.

## V. DISCUSSION

### A. Loss landscape seen by quantum search

We now argue that the quantum search is associated with a sequence of cost function landscapes with global minima only.

The key unitaries in Grover's search can be interpreted as evolution generated by kinetic and potential energy operators respectively [\[45\]](#). More specifically, in a notation similar to [Ref. \[45\]](#), the time evolution under Grover search is

$$|\psi(x, \tau)\rangle = (DR)\dots(DR)(DR)(DR)|\psi(x, 0)\rangle, \quad (23)$$

where  $D$  is the diffusion operator and  $R$  the Oracle.

$$D \equiv \begin{bmatrix} (1 - iN\epsilon) & i\epsilon & i\epsilon & \dots & i\epsilon \\ i\epsilon & (1 - iN\epsilon) & i\epsilon & \dots & i\epsilon \\ i\epsilon & i\epsilon & (1 - iN\epsilon) & \dots & i\epsilon \\ \vdots & \vdots & \vdots & \ddots & \vdots \\ i\epsilon & i\epsilon & i\epsilon & \dots & (1 - iN\epsilon) \end{bmatrix}, \quad \text{and } \epsilon$$

arises from discretizing the time in Grover search and is infinitesimal, defined by  $dx = \sqrt{\frac{dt}{\epsilon}}$ . Moreover,

$$R \equiv \begin{bmatrix} e^{-iV(x_1)dt} & 0 & 0 & \dots & 0 \\ 0 & e^{-iV(x_2)dt} & 0 & \dots & 0 \\ 0 & 0 & e^{-iV(x_3)dt} & \dots & 0 \\ \vdots & \vdots & \vdots & \ddots & \vdots \\ 0 & 0 & 0 & \dots & e^{-iV(x_N)dt} \end{bmatrix}.$$

Thus  $R = \exp(-i \sum_j V(x_j) |j\rangle\langle j| dt)$  is associated with the potential energy generator  $\sum_j V(x_j) |j\rangle\langle j|$  with potential energy landscape  $V(x_j)$ . The generator of  $D$  can then be interpreted as a discretized momentum operator  $T$  since  $DR$  arose from discretizing the Schroedinger equation generated by  $T + V$ . Thus the initial superposition state of Grover search can be interpreted as a superposition of initial positions, and the time evolution is the rolling down the hill  $V(x_j)$ . For Grover search

$V(x_j) \in \{0, -\pi\}$  with  $-\pi$  being the dip in the hill. For example, if the second state is marked and is thus the dip, then  $V = \text{diag}(0, -\pi, 0, 0, \dots)$ .

There is a sequence of potential energy landscapes associated with our NN training approach. In our NN training approach the threshold for which weight strings are awarded a  $\pi$  phase is gradually increased. Each threshold is associated with a given landscape, as depicted in Fig.9. These landscapes are, in line with the above, binary with any minima being global.

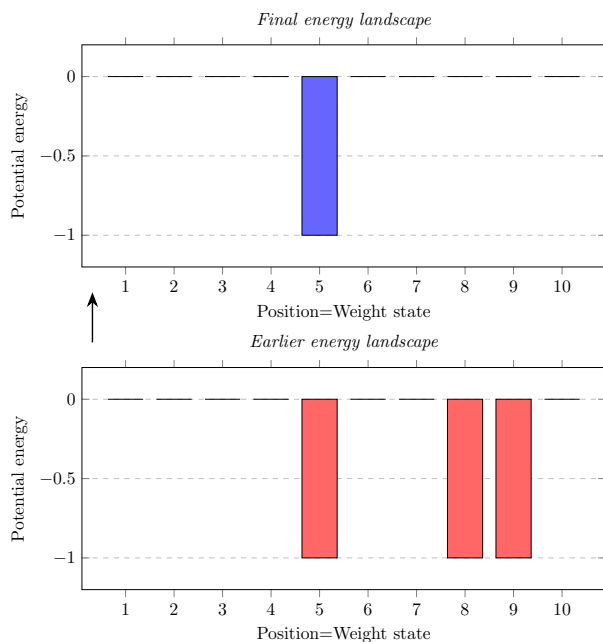


FIG. 9: **Energy landscapes associated with quantum search.** Marked elements correspond to global minima of potential energy. Each threshold for which elements are marked is associated with a different landscape, with successive landscapes having fewer and fewer global minima.

The physics corresponding to quantum search descent has two significant differences from the physics corresponding to classical gradient descent. Firstly, the quantum search starts in a quantum superposition of different positions, whereas classical gradient descent starts in a single location or probabilistic combination of locations. This quantum parallelism enables the system to converge to the state with the lowest ‘potential energy’ in  $O(\sqrt{N})$  time, where  $N$  is the number of positions. Secondly, the quantum search evolution has, if implemented faithfully physically, no energy dissipation, as it is generated by a time-independent Hamiltonian. In contrast, classical gradient descent can be interpreted as a dissipation of energy to a zero-temperature heat bath (or finite temperature heat bath in the case of simulated annealing) modeled via Monte Carlo evolution. This difference is

one way of understanding why the quantum search must be stopped at the right time, when the system is passing through the minimum, whereas classical gradient descent (at zero temperature) has a stable final point.

## B. Comparison between classical and quantum training time

Our quantum discrete sine neural network training is structured similarly to the quantum binary neural network training (QBNN) [40], so its complexity shares many similarities. In a binary neural network, where each weight takes one of two possible values (e.g. -1 or 1), there are  $2^M$  possible configurations for  $M$  weights. The complexity of a brute-force search to find the optimal binary weights grows exponentially with the number of weights. In classical training, the search requires  $N_C^{cl} = N \cdot 2^M$  calls, where  $N$  is the number of training data pairs.

For the quantum training method, since the number of “good” weights is not predetermined,  $O(\log(N/\delta))$  times of Grover’s search is required, where  $\delta$  is the precision needed to find an appropriate threshold  $\tau$  [40]. So  $O(\log(N/\delta)\sqrt{2^M})$  of Grover’s iterations are expected. Each iteration has  $O(1)$  phase estimations. The precision of phase estimation is  $O(1/N)$ , so the number of phase registers is  $O(\log N)$  and the number of controlled unitaries is  $O(N)$ . Each controlled unitary consists of  $O(N)$  feed-forward unitaries. In total, the complexity for the quantum training method is  $O(N^2 \log(N/\delta)\sqrt{2^M})$ .

The ratio between the classical brute-force search and quantum binary neural network training is:

$$\frac{N_C^{cl}}{N_C^{qm}} \approx \frac{2^{M/2}}{N \log(N/\delta)}. \quad (24)$$

To make the training process feasible, the ratio of the number of training data pairs  $N$  to the number of weights  $M$  should be balanced. Since  $M$  is typically large, the quantum algorithm often shows significant reductions in training time compared to a global classical search. We expect gradient descent training to be faster than our quantum training algorithm for large numbers of weights; however, it may yield less optimal results, such as getting trapped in local minima or experiencing vanishing gradients, as described in former sections, whereas the quantum training is guaranteed to reach the global minimum.

## VI. SUMMARY AND OUTLOOK

We analyze gradient descent training of sinusoidal neural networks (SinNN) and find that their loss landscape consists of multiple shallow local minima. When weights are initialized with different random seeds, they rarely

reach global minimum loss. A discretized sinusoidal neural network (DSinNN) is introduced and vanishing gradient problems are discovered. Finding optimal solutions for these non-convex problems is significantly challenging with gradient descent training and time-consuming for brute force search.

A quantum training algorithm is introduced to train the DSinNN model, which is guaranteed to find global optimal weight configurations. It evolves weights from equal probability superposition to the best weights with minimum training loss. We demonstrate this algorithm's performance on a toy DSinNN model with a classical simulation of 18 qubits. It overcomes the shallow local minima obstacles encountered by gradient descent and drastically improves brute force search time efficiency.

We believe that this constitutes an attractive potential use of quantum cloud computers. For practical applications one should investigate the possibility of minimizing the hardware resources required by trading off accuracy

and by optimizing the hardware resources used, e.g. minimizing the number of CNOT gates. Error correction and mitigation should similarly be investigated.

## ACKNOWLEDGMENTS

We thank Kaiming Bian, Feiyang Liu, Fei Meng, Maria Violaris and Ge Zhang for discussions. We acknowledge support from the City University of Hong Kong (Project No. 9610623).

## CODE AVAILABILITY

The codes implementing the quantum and classical trainings are available at [github.com/zw2788/Quantum-Sine-NN/](https://github.com/zw2788/Quantum-Sine-NN/).

- 
- [1] K. He, X. Zhang, S. Ren, and J. Sun, Delving deep into rectifiers: Surpassing human-level performance on imagenet classification, in *Proceedings of the IEEE International Conference on Computer Vision (ICCV)* (IEEE, 2015) pp. 1026–1034.
- [2] W. Xiong, L. Wu, F. Alleva, J. Droppo, X. Huang, and A. Stolcke, *The Microsoft 2017 Conversational Speech Recognition System Technical Report*, Report MSR-TR-2017-39, (2017).
- [3] A. Vaswani, Attention is all you need, *Advances in Neural Information Processing Systems* **30** (2017).
- [4] M. Bojarski, D. Del Testa, D. Dworakowski, B. Firner, B. Flepp, P. Goyal, L. D. Jackel, M. Monfort, U. Muller, J. Zhang, X. Zhang, J. Zhao, and K. Zieba, *End to end learning for self-driving cars*, arXiv preprint arXiv:1604.07316 (2016).
- [5] D. Ribli, A. Horváth, Z. Unger, P. Pollner, and I. Csabai, Detecting and classifying lesions in mammograms with deep learning, *Scientific Reports* **8**, 4165 (2018).
- [6] Y. LeCun, Y. Bengio, and G. Hinton, Deep learning, *Nature* **521**, 436 (2015).
- [7] D. E. Rumelhart, G. E. Hinton, and R. J. Williams, Learning representations by back-propagating errors, *Nature* **323**, 533 (1986).
- [8] X. Glorot, A. Bordes, and Y. Bengio, Deep sparse rectifier neural networks, *Proceedings of the fourteenth international conference on artificial intelligence and statistics, JMLR* **15**, 315 (2011).
- [9] D.-A. Clevert, Fast and accurate deep network learning by exponential linear units (elus), arXiv preprint arXiv:1511.07289 (2015).
- [10] A. L. Maas, A. Y. Hannun, A. Y. Ng, *et al.*, Rectifier nonlinearities improve neural network acoustic models, in *Proceedings of the 30th International Conference on Machine Learning*, Vol. 30 (Atlanta, GA, 2013) p. 3.
- [11] D. Hendrycks and K. Gimpel, Gaussian error linear units (gelus), arXiv preprint arXiv:1606.08415 (2016).
- [12] S. Elfving, E. Uchibe, and K. Doya, Sigmoid-weighted linear units for neural network function approximation in reinforcement learning, *Neural networks* **107**, 3 (2018).
- [13] Gallant, There exists a neural network that does not make avoidable mistakes, in *IEEE 1988 International Conference on Neural Networks* (IEEE, 1988) pp. 657–664.
- [14] M. Uteuliyeva, A. Zhumekenov, R. Takhanov, Z. Assylbekov, A. J. Castro, and O. Kabdolov, Fourier neural networks: A comparative study, *Intelligent Data Analysis* **24**, 1107 (2020).
- [15] K. Wong, C. Leung, and S. Chang, Handwritten digit recognition using multilayer feedforward neural networks with periodic and monotonic activation functions, in *2002 International Conference on Pattern Recognition*, Vol. 3 (IEEE, 2002) pp. 106–109.
- [16] G. Parascandolo, H. Huttunen, and T. Virtanen, Taming the waves: sine as activation function in deep neural networks, in *URL https://openreview.net/forum* (2016).
- [17] R. Koplon and E. D. Sontag, Using Fourier-neural recurrent networks to fit sequential input/output data, *Neurocomputing* **15**, 225 (1997).
- [18] M. H. Choueiki, C. A. Mount-Campbell, and S. C. Ahalt, Implementing a weighted least squares procedure in training a neural network to solve the short-term load forecasting problem, *IEEE Transactions on Power systems* **12**, 1689 (1997).
- [19] P. Liu, Z. Zeng, and J. Wang, Multistability of recurrent neural networks with nonmonotonic activation functions and mixed time delays, *IEEE Transactions on Systems, Man, and Cybernetics: Systems* **46**, 512 (2015).
- [20] V. Sitzmann, J. Martel, A. Bergman, D. Lindell, and G. Wetzstein, Implicit neural representations with periodic activation functions, *Advances in neural information processing systems* **33**, 7462 (2020).
- [21] I. Hubara, M. Courbariaux, D. Soudry, R. El-Yaniv, and Y. Bengio, Binarized neural networks, *Advances in neural information processing systems* **29** (2016).
- [22] H. Qin, R. Gong, X. Liu, X. Bai, J. Song, and N. Sebe, Binary neural networks: A survey, *Pattern Recognition* **105**, 107281 (2020).

- [23] M. Rastegari, V. Ordonez, J. Redmon, and A. Farhadi, Xnor-net: Imagenet classification using binary convolutional neural networks, in *Computer Vision – ECCV 2016* (Springer International Publishing) pp. 525–542.
- [24] A. Gholami, S. Kim, Z. Dong, Z. Yao, M. W. Mahoney, and K. Keutzer, A survey of quantization methods for efficient neural network inference, in *Low-Power Computer Vision* (Chapman and Hall/CRC, 2022) pp. 291–326.
- [25] M. Nagel, M. Fournarakis, R. A. Amjad, Y. Bondarenko, M. Van Baalen, and T. Blankevoort, A white paper on neural network quantization, arXiv preprint arXiv:2106.08295 (2021).
- [26] G. Swirszcz, W. M. Czarnecki, and R. Pascanu, Local minima in training of neural networks, arXiv preprint arXiv:1611.06310 [10.48550/arXiv.1611.06310](https://arxiv.org/abs/1611.06310) (2016).
- [27] L. Ziyin, T. Hartwig, and M. Ueda, Neural networks fail to learn periodic functions and how to fix it, *Advances in Neural Information Processing Systems* **33**, 1583 (2020).
- [28] K. H. Wan, O. Dahlsten, H. Kristjánsson, R. Gardner, and M. S. Kim, Quantum generalisation of feedforward neural networks, *npj Quantum Information* **3**, 36 (2017).
- [29] I. Cong, S. Choi, and M. D. Lukin, Quantum convolutional neural networks, *Nature Physics* **15**, 1273 (2019).
- [30] K. Beer, D. Bondarenko, T. Farrelly, T. J. Osborne, R. Salzmann, D. Scheiermann, and R. Wolf, Training deep quantum neural networks, *Nature Communications* **11**, 808 (2020).
- [31] A. Abbas, D. Sutter, C. Zoufal, A. Lucchi, A. Figalli, and S. Woerner, The power of quantum neural networks, *Nature Computational Science* **1**, 403 (2021).
- [32] M. Larocca, N. Ju, D. García-Martín, P. J. Coles, and M. Cerezo, Theory of overparametrization in quantum neural networks, *Nature Computational Science* **3**, 542 (2023).
- [33] E. R. Anschuetz, H.-Y. Hu, J.-L. Huang, and X. Gao, Interpretable quantum advantage in neural sequence learning, *PRX Quantum* **4**, 020338 (2023).
- [34] J. R. McClean, S. Boixo, V. N. Smelyanskiy, R. Babush, and H. Neven, Barren plateaus in quantum neural network training landscapes, *Nature Communications* **9**, 4812 (2018).
- [35] Y. Liao, M.-H. Hsieh, and C. Ferrie, Quantum optimization for training quantum neural networks, *Quantum Machine Intelligence* **6**, 33 (2024).
- [36] C.-Y. Liu, E.-J. Kuo, C.-H. A. Lin, S. Chen, J. Gem-sun Young, Y.-J. Chang, and M.-H. Hsieh, [Training classical neural networks by quantum machine learning](https://arxiv.org/abs/2402.16465) (2024), [arXiv:2402.16465 \[quant-ph\]](https://arxiv.org/abs/2402.16465).
- [37] Y. Du, M.-H. Hsieh, T. Liu, and D. Tao, A grover-search based quantum learning scheme for classification, *New Journal of Physics* **23**, 023020 (2021).
- [38] L. K. Grover, A fast quantum mechanical algorithm for database search, in *Proceedings of the Twenty-Eighth Annual ACM Symposium on Theory of Computing*, STOC '96 (Association for Computing Machinery, 1996) p. 212–219.
- [39] M. Ganger, W. Hu, *et al.*, Quantum multiple q-learning, *International Journal of Intelligence Science* **9**, 1 (2019).
- [40] Y. Liao, D. Ebler, F. Liu, and O. Dahlsten, Quantum speed-up in global optimization of binary neural nets, *New Journal of Physics* **23**, 063013 (2021).
- [41] A. Y. Kitaev, Quantum measurements and the abelian stabilizer problem, arXiv preprint [quant-ph/9511026](https://arxiv.org/abs/quant-ph/9511026) (1995).
- [42] M. Boyer, G. Brassard, P. Høyer, and A. Tappa, Tight bounds on quantum searching, in *Quantum Computing* (1999) pp. 187–199.
- [43] D. Oliveira and R. Ramos, Quantum bit string comparator: Circuits and applications, *Quantum Computers and Computing* **7** (2007).
- [44] J. R. Johansson, P. D. Nation, and F. Nori, Qutip: An open-source python framework for the dynamics of open quantum systems, *Computer Physics Communications* **183**, 1760 (2012).
- [45] L. K. Grover, From Schrödinger’s equation to the quantum search algorithm, *Pramana* **56**, 333 (2001).